

RESEARCH

Open Access



# The gut-liver axis plays a limited role in mediating the liver's heat susceptibility of Chinese giant salamander

Runliang Zhai<sup>1,4†</sup>, Chunlin Zhao<sup>2†</sup>, Liming Chang<sup>1,4†</sup>, Jiongyu Liu<sup>1,4</sup>, Tian Zhao<sup>3\*</sup>, Jianping Jiang<sup>1,4\*</sup> and Wei Zhu<sup>1,4\*</sup>

## Abstract

The Chinese giant salamander (CGS, *Andrias davidianus*), a flagship amphibian species, is highly vulnerable to high temperatures, posing a significant threat under future climate change. Previous research linked this susceptibility to liver energy deficiency, accompanied by shifts in gut microbiota and reduced food conversion rates, raising questions about the role of the gut-liver axis in mediating heat sensitivity. This study investigated the responses of Chinese giant salamander larvae to a temperature gradient (10–30 °C), assessing physiological changes alongside histological, gut metagenomic, and tissue transcriptomic analyses. Temperatures above 20 °C led to mortality, which resulted in delayed growth. Histological and transcriptomic data revealed metabolic exhaustion and liver fibrosis in heat-stressed salamanders, underscoring the liver's critical role in heat sensitivity. While heat stress altered the gut microbiota's community structure, their functional profiles, especially in nutrient absorption and transformation, remained stable. Both gut and liver showed temperature-dependent transcriptional changes, sharing some common variations in actins, heat shock proteins, and genes related to transcription and translation. However, their energy metabolism exhibited opposite trends: it was downregulated in the liver but upregulated in the gut, with the gut showing increased activity in the pentose phosphate pathway and oxidative phosphorylation, potentially countering metabolic exhaustion. Our findings reveal that the liver of the larvae exhibits greater thermal sensitivity than the gut, and the gut-liver axis plays a limited role in mediating thermal intolerance. This study enhances mechanistic understanding of CGS heat susceptibility, providing a foundation for targeted conservation strategies in the face of climate change.

**Keywords** Conservation, Metabolic exhaustion, Microbiota, Salamander, Temperature

<sup>†</sup>Runliang Zhai, Chunlin Zhao and Liming Chang contributed equally to this work.

\*Correspondence:  
Tian Zhao  
owfaowfa@swu.edu.cn  
Jianping Jiang  
jiangjp@cib.ac.cn

Wei Zhu  
zhuwei@cib.ac.cn  
<sup>1</sup>Chengdu Institute of Biology, Chinese Academy of Sciences, Chengdu 610213, China  
<sup>2</sup>School of Biological and Chemical Engineering, School of Agriculture, Panzhihua University, Panzhihua 617000, China  
<sup>3</sup>College of Fisheries, Southwest University, Chongqing 400715, China  
<sup>4</sup>University of Chinese Academy of Sciences, Beijing 101408, China



## Introduction

Warming poses a significant threat to the health and productivity of animals, especially ectotherms [1, 2]. Among vertebrates, amphibians are particularly vulnerable to environmental changes due to their complex life cycles and highly permeable skin, leading to a global threat to 40.7% of species [3]. Warming is widely recognized as a major factor driving the ongoing decline of wild amphibian populations [4–6]. Therefore, a thorough understanding of the physiological and biochemical mechanisms by which heat stress impacts amphibians is essential for their conservation [7, 8].

The Chinese giant salamander (CGS, *Andrias davidianus*), one of the largest extant amphibian species, is a flagship species in amphibian conservation [9, 10]. This species belongs to a lineage that dates back approximately 200 million years, making it one of the oldest surviving amphibian species and earning it the distinction of a living fossil [11]. Historically, CGS was widely distributed across central and southern China [12, 13]; however, wild populations have dramatically declined in recent decades due to habitat degradation, pollution, and overexploitation [14, 15]. The species is currently classified as Critically Endangered [16]. Despite successes in artificial breeding, efforts to restore wild populations have limited success, even with significant translocation efforts of farmed individuals into their historical natural habitats [17]. In this context, advancing research on the physiological characteristics of CGS larvae could be pivotal in overcoming the current conservation challenges. Temperature has been identified as a key environmental factor influencing the physiological performance of CGS [18–21]. While larvae exhibits notable cold tolerance [22], it is highly susceptible to elevated temperatures, particularly those exceeding 20 °C. Such temperatures have been shown to decrease feeding activity, accelerate development, suppress somatic growth, and increase mortality [18, 23–26]. Future climate warming is likely to reduce their adult body size and threaten their survival [14, 27]. This makes CGS an important model for studying how heat stress impacts amphibians.

Heat stress can lead to functional disability, metabolic exhaustion, oxidative damage, immune suppression, and accelerated aging in animals [28]. However, different organs may exhibit varying degrees of responsiveness and susceptibility to temperature changes [22, 29]. Our previous research has shown that the liver in larvae is more severely impacted by heat stress (25 °C, water temperature) compared to other organs, such as the brain, heart, gills, skin, limbs, and tail. This is characterized by morphological enlargement, energy deficiency, and a reduction in protein levels in the liver, along with the shortening of the tail, an essential fat storage organ [23]. Given the liver's central role in maintaining whole-body

metabolic homeostasis and producing plasma proteins, its energy deficiency is likely a key contributor to the overall decline in organismal fitness [23]. While impaired glycogen metabolism contributes to hepatic energy deficiency under heat stress, whether interactions with nutrient-absorbing organs, particularly the gut, play a role in this metabolic exhaustion remains unclear.

The gut-liver axis plays a critical role in maintaining overall health, metabolic homeostasis, and immune function, with the gut microbiota being a key component of this relationship [30, 31]. The gut microbiota influences the host's gut by aiding in nutrient breakdown and absorption, as well as producing metabolites and signaling molecules that affect metabolism [32–35]. The gut impacts the liver through the absorption of nutrients, microbial metabolites, and endotoxins [36]. Understanding the role of this axis in animal thermal sensitivity is important, as the plasticity and colonization potential of the gut microbiota present a promising opportunity to manipulate animals' thermal physiological performance [37–39]. Our previous research demonstrated that heat stress (25 °C, water temperature) significantly altered the gut microbiota of larvae, reducing their alpha-diversity and disrupting their community structure [21]. Additionally, we observed a marked decrease in the food conversion rate in heat-stressed larvae [23]. This could be attributed to increased maintenance energy costs (e.g., maintaining ion gradients) at elevated temperatures [20, 40]. However, the possibility of impaired gut development or reduced gut metabolic activity and function at higher temperatures cannot be excluded. Based on these findings, we hypothesize that heat-induced changes in gut microbiota and gut function may act as upstream events leading to metabolic exhaustion in the liver via the gut-liver axis.

In this study, we established a thermal gradient (10, 15, 20, 25, and 30 °C) to investigate the role of the gut-liver axis in the heat susceptibility of the larvae, with a specific focus on the Shanxi clade. We employed a combination of histological analysis, metagenomics, and multi-organ transcriptomics to investigate whether heat-induced changes in the gut and its associated microbiota are connected to impaired liver function under heat stress. To support our hypothesis, we anticipate the following outcomes in heat-stressed individuals: (1) A significant shift in gut microbial functions, particularly those related to nutrient breakdown and absorption; (2) Notable histological and transcriptional changes in both the gut and liver; and (3) Parallel trends in metabolic variations, indicating signs of metabolic exhaustion, between the liver and gut (Fig. 1a).

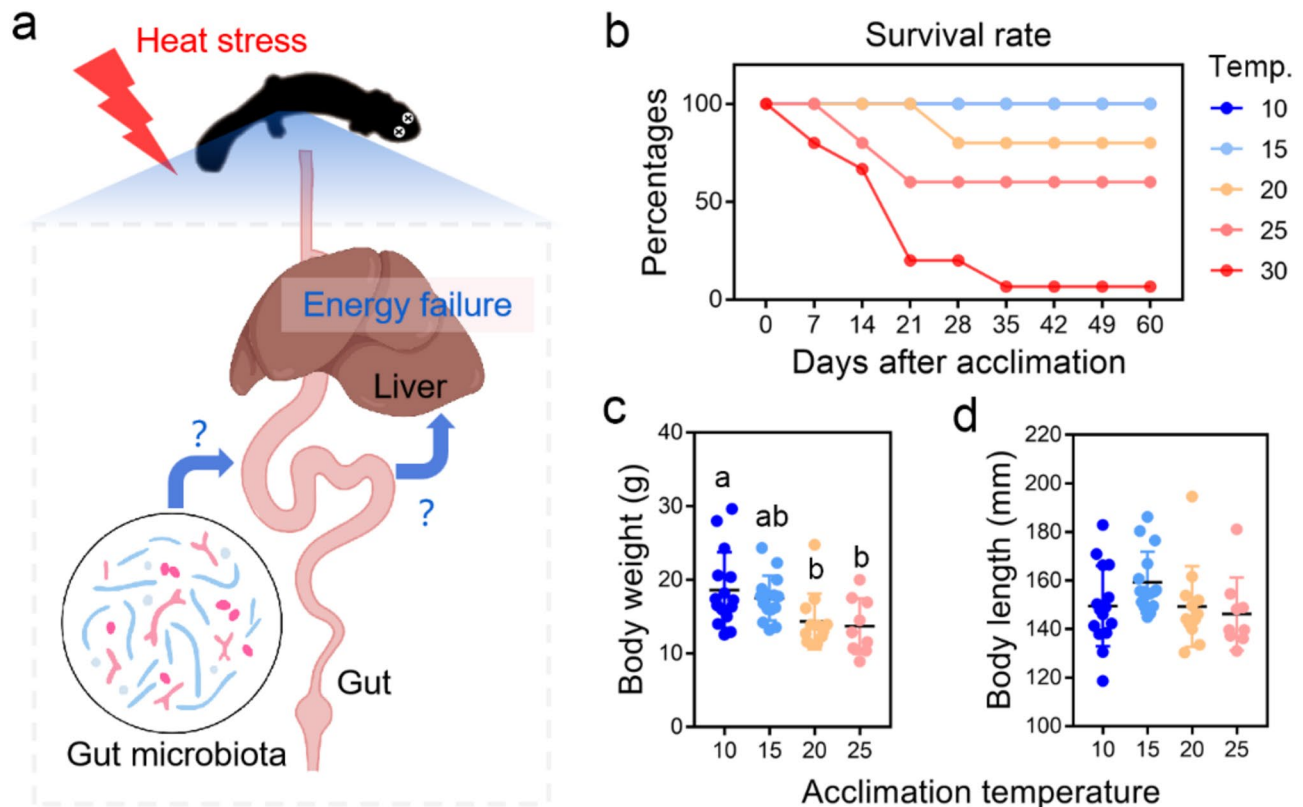


**Fig. 1** Impact of heat stress on CGS. **(a)** Study hypothesis. **(b)** Survival rate of CGS at different acclimation temperatures. **(c–d)** Variations in body weight and length at the end of the experiment. Different letters indicate significant differences ( $p < 0.05$ ) between groups, as determined by one-way ANOVA followed by the S-N-K post hoc test

## Materials and methods

### Animals and thermal acclimation

Larvae of the Chinese giant salamander (Shanxi clade, 370 days of age, body weight =  $16.9 \pm 0.54$  g) were collected from a semi-natural aquaculture farm ( $102^{\circ}10'05''$  E,  $29^{\circ}52'36''$  N) located in Hongya County, Sichuan Province, China, where the water temperature was maintained between 13 and 17 °C [22]. Through comparative analysis of the mitochondrial CO1 sequence, we have confirmed that these individuals belong to the Shanxi clade, one of the most representative clades of CGS. In the laboratory, these larvae were kept at  $17 \pm 1.2$  °C (air temperature) and fed red worms (*Chironomus* sp. larvae). The photoperiod was set to 12 L: 12D. After a 28-day acclimation to laboratory conditions, the larvae were randomly divided into five groups ( $n = 15$  larvae per group), each acclimated to different temperature settings: 10/10.8 °C, 15/16.4 °C, 20/22.3 °C, 25/24.1 °C, and 30/28.1 °C (set air/actual water temperature) in five climate chambers, while other conditions remained unchanged. The 10 °C and 15 °C conditions fall within the optimal thermal range, while the other temperatures are considered stressful to CGS. Each group was housed in three plastic containers (35 cm  $\times$  25 cm  $\times$  15 cm, with a water level of 5 cm), representing three independent replicates. Thermal acclimation

lasted for 60 days, during which the water was changed, and the larvae were fed sufficient red worms every third day. Mortality rates were recorded daily, and the body weight of the larvae was measured at the end of the experiment. Following the 60-day thermal acclimation period, the larvae received intraperitoneal injections of 0.5 mL physiological saline (as a control for another experiment) and were returned to their respective temperature conditions for three hours. The larvae were then euthanized using MS-222, and the liver, gut, and gut contents were collected. All animal protocols in this study were reviewed and approved by the Animal Ethical and Welfare Committee of the Chengdu Institute of Biology, Chinese Academy of Sciences (permit number: CIBDWLL2023013), in compliance with the ARRIVE guidelines 2.0 [41] and Guide for the Care and Use of Laboratory Animals (8th edition) published by National Research Council (US) Committee for the Update of the Guide for the Care and Use of Laboratory Animals [42].

### Histological section

The tissue samples were stored in 4% paraformaldehyde until histological analysis. Following dehydration in a graded series of ethanol and clearing with xylene, the livers were embedded in paraffin and sectioned into serial

transverse Sect. (7  $\mu\text{m}$  thick). Hematoxylin and eosin (H & E) staining was performed to reveal the general histological characteristics.

### Metagenomic analyses

The gut contents of the larvae were collected for metagenomic analysis, with a total of 6, 6, 6, and 4 samples randomly selected from the 10, 15, 20, and 25  $^{\circ}\text{C}$  groups, respectively. Total genomic DNA was extracted using the Zymo Research BIOMICS DNA Microprep Kit (Zymo Research Co., U.S.). The nucleic acid concentration was measured using the Tecan F200 (Tecan Co., Switzerland) with the PicoGreen assay. DNA fragmentation was carried out using the Covaris M220 (Covaris Co., U.S.), and libraries were prepared with the NEBNext<sup>®</sup> Ultra<sup>™</sup> II DNA Library Prep Kit for Illumina<sup>®</sup> and NEBNext<sup>®</sup> Multiplex Oligos for Illumina<sup>®</sup> (Dual Index Primers Set 1) (New England Biolabs Co., U.S.). Library quality was assessed using the Agilent 2100 Bioanalyzer system (Agilent Technologies Inc., U.S.), and library concentration was determined via qPCR. Sequencing was conducted on the Illumina NovoSeq 6000 platform (Rhonin Biosciences, China). The raw sequencing data were deposited in the Genome Sequence Archive (GSA) under the accession number CRA018593 [43, 44].

Raw sequences were processed with Trimmomatic to remove low-quality bases and sequencing adapters [45]. Quality assessments were performed on the sequences before and after trimming using fastQC and MultiQC [46, 47]. Sequence assembly for each sample was conducted using Megahit [48], and the assembled sequences were evaluated for quality using Quast [49]. Gene prediction on the assembled contigs was performed using Prodigal [50]. All genes across samples were pooled, and gene set dereplication was carried out using MMseq2 (with a coverage threshold of 80% and similarity threshold of 90%) [51]. The Burrows-Wheeler Alignment Tool was used to map the clean reads back to the non-redundant gene set, enabling the evaluation of sequence counts for each non-redundant gene in each sample and subsequent gene quantification [52]. Functional annotation of the non-redundant gene set was performed using databases such as NR, EggNOG, KEGG, CAZy, CARD, VFDB, and Phi [53–59]. Community structure analysis was conducted using Kraken based on the RefSeq database [60, 61].

### Transcriptomic analyses

The gut and liver tissues were collected for total RNA extraction using the TRIzol reagent according to the manufacturer's protocol (Life Technologies Corp., Carlsbad, CA, USA). A total of 5, 5, 5, and 4 liver or gut samples were collected from the 10, 15, 20, and 25  $^{\circ}\text{C}$  groups, respectively. Subsequently, 1  $\mu\text{g}$  of RNA from each

sample was utilized for library construction by employing the NEBNext<sup>®</sup>Ultra<sup>™</sup> RNA Library Prep Kit for Illumina<sup>®</sup> (NEB, USA). After cluster generation, the library preparations were sequenced on an Illumina HiSeq 6000 platform by Biomarker Technologies Co. Ltd., and paired-end reads were generated. The raw sequencing data were deposited in the Genome Sequence Archive (GSA) under the accession number CRA016012. Read quality was assessed using FastQC v0.11.9 and summarized with MultiQC v1.9. Trimming was performed with Trimmomatic v0.39, and genome alignment was carried out using FastQ Screen v0.15.2 with Bowtie2 v2.4.1 [62]. De novo transcriptome assembly was conducted with Trinity v2.11.0 [63]. Clusters and gene-level counts of the transcriptome were obtained using Corset v1.09 and Salmon v1.3.0 [64, 65]. Assembly quality was evaluated with QUAST v5.1.0rc1 and BUSCO v4.1.4 against the eukaryota\_odb10 database [66]. Read representation was assessed using Bowtie2. The Trinotate v3.2.1 pipeline was used for biological data annotation, employing three custom reference sub-databases: Swiss-Prot (all vertebrates), TrEMBL (all vertebrates), and NR (Amphibia), for BLAST homology searches using DIAMOND v2.0.15. Gene expression levels were presented as transcripts per million (TPM) values, calculated using Salmon.

### Statistical analyses

Basic statistical analyses were conducted using IBM SPSS v21.0 (IBM, Armonk, NY, USA) and R [67]. The Kolmogorov-Smirnov and Shapiro-Wilk tests were employed to assess whether the data significantly deviated from a normal distribution, and Levene's tests were conducted to evaluate homoscedasticity across groups. Intergroup differences in CGS body traits and gut microbial alpha-diversity were examined using one-way ANOVA followed by post hoc S-N-K tests. Bray-Curtis distances were calculated to represent the dissimilarity in microbial community structure, microbial metagenomes, and tissue gene expression profiles [68]. Principal coordinates analysis (PCoA) was used to visualize these dissimilarities, and PERMANOVA was conducted to test for intergroup differences in these dissimilarities [68]. LEfSe analysis was performed to identify differential microbial taxa between thermal groups [69]. For metagenomic analyses, one-way ANOVA was used to examine intergroup differences in the relative abundance of microbial functional genes or pathways. In tissue transcriptomic analyses, significantly differentially expressed genes (DEGs) across thermal groups were identified using a stringent criterion of adjusted  $p < 0.01$  after one-way ANOVA with Benjamini and Hochberg's (BH) correction. TCseq was used to analyze the temperature-dependent expression patterns of DEGs [70]. Gene enrichment analysis was conducted using the KEGG database via KOBAS-i (<http://b>

[ioinfo.org/kobas](https://ioinfo.org/kobas)) with an adjusted  $p < 0.001$  [71]. Graphs were generated using GraphPad Prism 5, clusterProfiler 4.0, and ggplot2 [72].

## Results

During the acclimation period, mortality was observed at temperatures as low as 20 °C, with mortality rates progressively increasing at higher temperatures (Fig. 1b). Most mortality occurred within the first thirty days of thermal acclimation. Even in the highest temperature group, no deaths were observed among surviving individuals during the last thirty days, highlighting individual differences in heat tolerance. CGS exposed to heat stress (20 and 25 °C) showed a declining trend in growth performance compared to those kept within the optimal temperature range (10 and 15 °C; Fig. 1c–d).

### Variations in gut microbiota

We investigated the influence of heat stress on gut microbial diversity and function. The dominant microbial taxa in the gut of CGS include Bacillota, Pseudomonadota, Actinomycetota, Verrucomicrobiota, and Bacteroidota at the phylum level (Fig. 2a), and *Akkermansia*, *Citrobacter*, *Flavonifractor*, and *Bacteroides* at the genus level (Fig. 2b). Heat stress reduced the microbial Shannon index and caused a shift in microbial community structure, with significant differences observed between individuals at 10 °C and 25 °C ( $p < 0.05$ , PERMANOVA; Fig. 2c–e). Differential analyses revealed that heat stress led to a decrease in the relative abundance of Actinomycetota, Micrococcaceae, Corynebacterium, Actinomycetaceae, and *Cellulomonas* ( $p < 0.05$  and LDA score  $> 3$ , LEfSe; Fig. 2f–g).

We further investigated changes in the gut metagenome under heat stress. A total of 1,722,575 unigenes were identified across the samples, with their functions annotated by querying public databases (Fig. 3a). Differential analyses revealed that heat stress significantly altered the unigene profile of the gut microbiota (Fig. 3b), with a notable difference observed between the 25 °C group and the 10 °C/15 °C groups ( $p < 0.05$ , PERMANOVA; Fig. 3c). To enhance functional interpretation, we streamlined the unigene data by merging unigenes with the same function, based on NR and KEGG Class 3 annotations. This process produced a functional gene abundance table and a functional pathway abundance table, offering a more accurate reflection of the metagenomes' functional profile. In contrast to the unigene profile results, the impact of heat stress on these functional profiles was less pronounced, with no significant differences ( $p > 0.05$ , PERMANOVA) detected in pairwise comparisons (Figs. 3d–e). Differential analyses indicated that heat stress did not affect the abundance of primary metabolic pathways (KEGG class 3; Fig. 3f), and

the relative abundance of microbial pathways involved in nutrient absorption and short-chain fatty acid (SCFA) production remained comparable across gut metagenomes from different groups ( $p > 0.05$ , one-way ANOVA; Figs. 3g–h).

### Histological changes in the gut and liver under heat stress

Heat stress induced histological changes in the liver but not in the gut (Fig. 4a). As the temperature increased, liver tissue exhibited a reduction in hepatocyte size, which was attributed to fewer and smaller intracellular vacuoles, representing lipid droplets in H&E sections. Moreover, hepatocytes in the 25 °C group showed significant morphological abnormalities, characterized by a strip-like, compressed cellular arrangement.

### Variations in the gene expression profile in the gut and liver

Heat stress induced a temperature-dependent shift in the transcriptional profiles of both gut and liver tissues (Fig. 4b and S1), with significant pairwise differences consistently observed between the control and heat-stressed groups ( $p < 0.05$ , PERMANOVA; Fig. 4c). The differentially expressed genes (DEGs) (adjusted  $p < 0.01$ , one-way ANOVA with BH correction) were grouped into six clusters based on distinct temperature-dependent expression patterns (Fig. 4d). In clusters 1 and 4, DEGs exhibited increased transcription with rising temperatures, while those in cluster 3 showed decreased transcription. The numbers of upregulated and downregulated DEGs under heat stress were comparable in the gut (down: up = 1,277: 1,186); however, in the liver, downregulated DEGs significantly outnumbered upregulated ones (down: up = 2,075: 348; Fig. 4e). A large proportion of downregulated DEGs were shared by both the gut and liver, indicating some common responses to heat stress between these organs (Fig. 4f). In contrast, only a small proportion of upregulated DEGs were shared between the gut and liver, highlighting organ heterogeneity in heat-induced gene transcriptional activation in CGS.

### Metabolic reorganization in the gut and liver under heat stress

Enrichment analyses were conducted to elucidate the functions of these DEGs. The gut and liver shared many of the pathways enriched by their respective upregulated DEGs, with notably higher enrichment rates observed in the gut (Fig. 5a). Actins played central roles in the subnetworks shared by the liver and gut (Figure S2). These genes were upregulated under heat stress in both organs, driving the enrichment of multiple cellular processes and primarily contributing to the convergence of enriched pathways between the gut and liver. Other upregulated pathways shared by the liver and gut included several

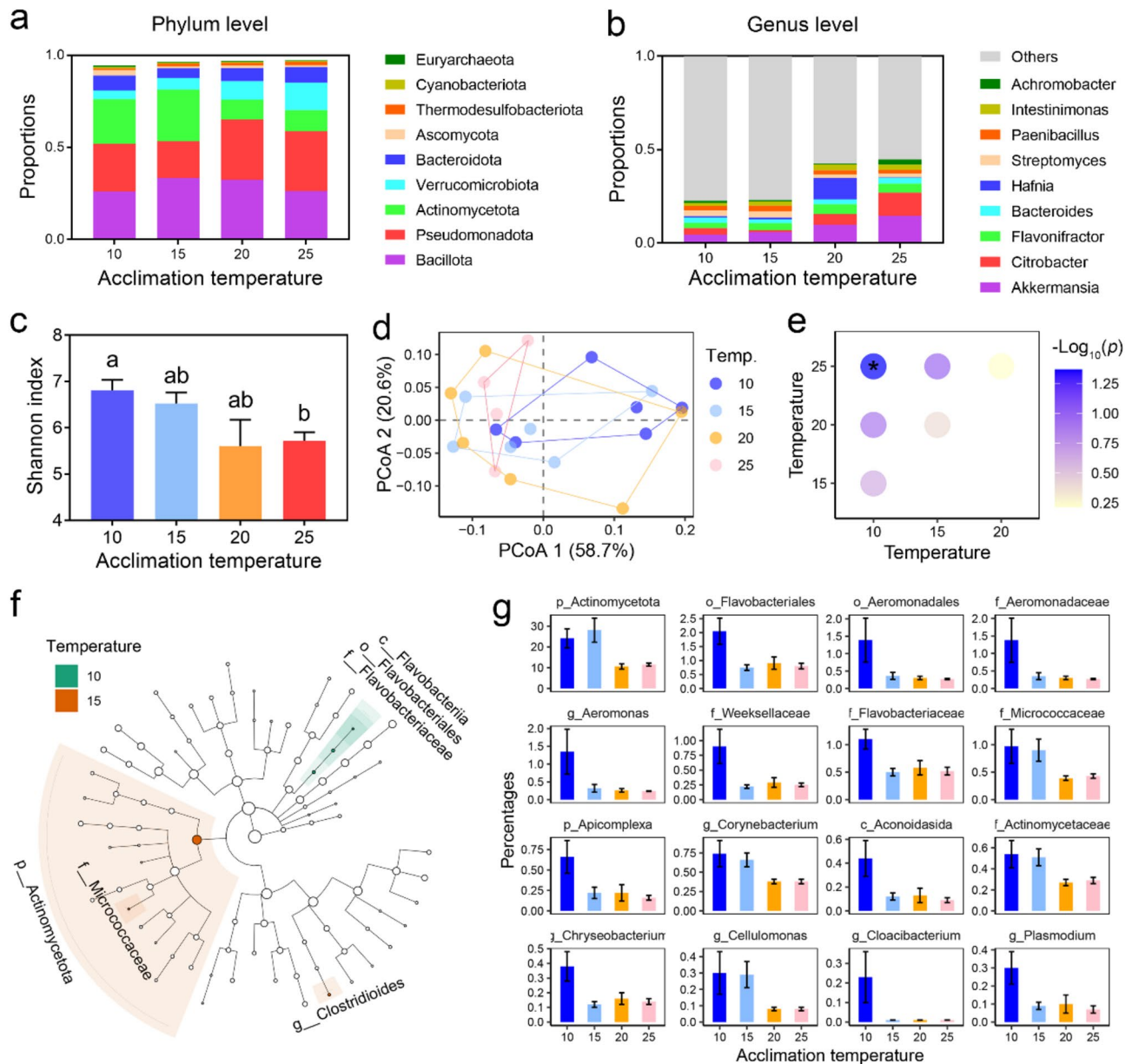


**Fig. 2** Effects of heat stress on gut microbial diversity in CGS. **(a–b)** Microbial composition at the phylum **(a)** and genus **(b)** levels. **(c)** Variations in microbial alpha-diversity between groups. Different letters indicate significant differences ( $p < 0.05$ ) between groups, as determined by Kruskal-Wallis test followed by the S-N-K post hoc test. **(d–e)** Variations in microbial beta-diversity between groups. The PCoA scatter plot **(d)** illustrates the similarity in microbial composition between samples. The heatmap **(e)** presents the statistical results of PERMANOVA on microbial beta-diversity (Bray-Curtis distances). Asterisks indicate significant differences between groups ( $p < 0.05$ ; pairwise PERMANOVA). **(f)** Results of LefSe analysis across the four temperatures. Note that featured bacterial taxa were only identified for 10 and 15 °C groups. This is because LefSe is a type of feature analysis method that identifies elements with higher abundance in one group compared to others. As a result, when multiple groups are involved, certain groups may fail to exhibit characteristic features due to their similarity to other groups or because they lie between the two other groups. **(g)** Variations in the relative abundance of differential microbial taxa with LDA scores  $> 3$  and  $p < 0.05$

key steps of the central dogma, such as RNA transport, the spliceosome, and the ribosome. From a metabolic perspective, although thermogenesis, a pathway encompassing oxidative phosphorylation (OPP), was enriched in both organs, this enrichment was driven by the transcriptional upregulation of OPP genes exclusively in the gut (Figure S2). Additionally, the gut exhibited

transcriptional upregulation of pathways related to carbon metabolism, as well as fructose and mannose metabolism, under heat stress (Fig. 5a–b).

For the enrichment analyses based on downregulated DEGs, the pathways shared by both organs included RNA transport, RNA degradation, mRNA surveillance, the spliceosome, protein processing in the endoplasmic

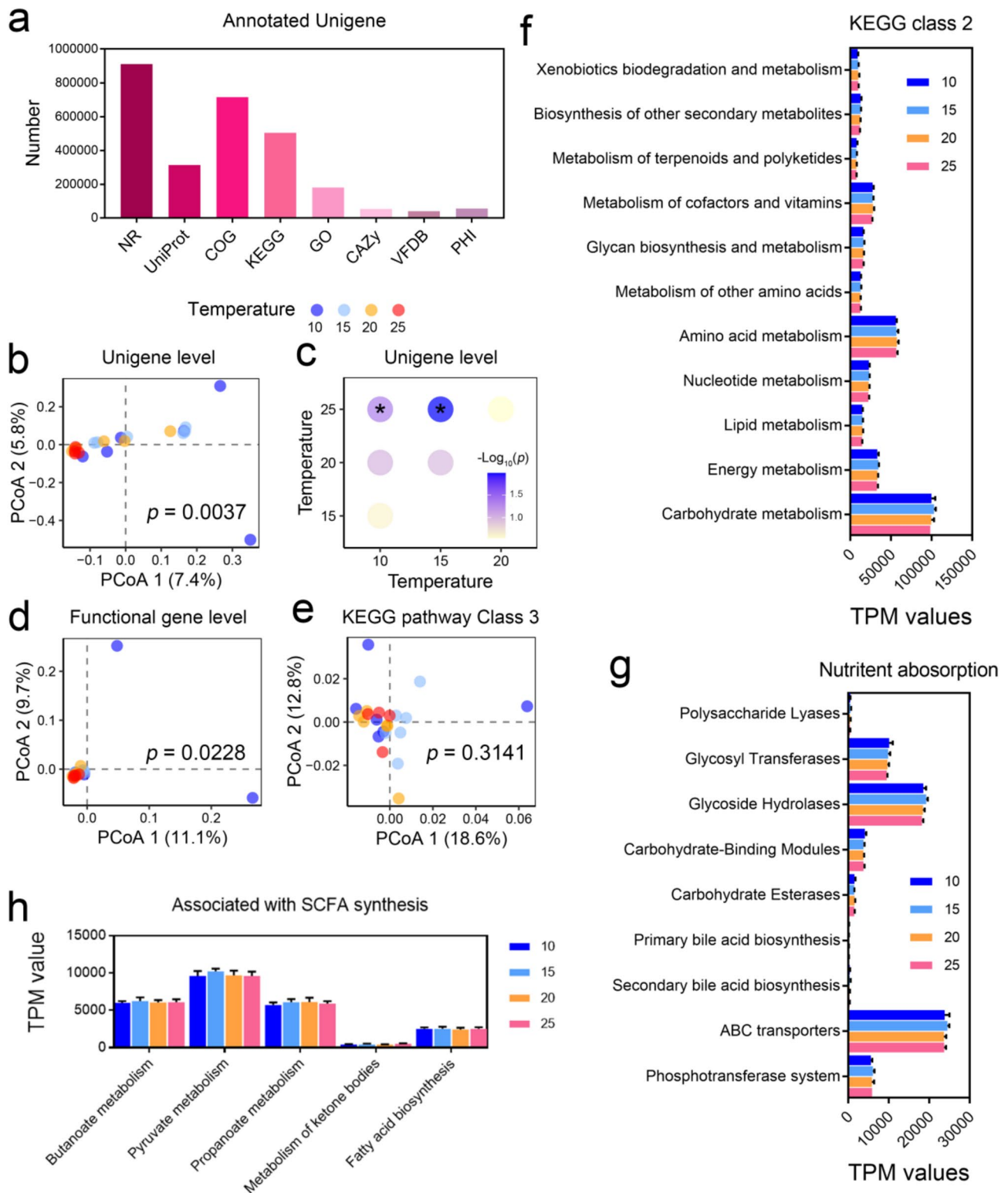


**Fig. 3** Functional variations in gut microbiota. **(a)** Summary of the annotation of unigenes. **(b)** PCoA of the metagenome profile at the unigene level. **(c)** Heatmap showing the statistical results of PERMANOVA on the metagenome (Bray-Curtis distances). Asterisks indicate significant differences between groups ( $p < 0.05$ ; pairwise PERMANOVA). **(d–e)** PCoA of the metagenome profile at the gene function level **(d)** and the functional pathway level (KEGG class 3) **(e)**. **(f–h)** Comparison of the abundance of functional pathways between groups: KEGG metabolic pathways at the class 2 level **(f)**, metabolic pathways related to nutrient absorption (KEGG class 3 and CAZY modules, **g**), and metabolic pathways related to SCFA synthesis (KEGG class 3, **h**)

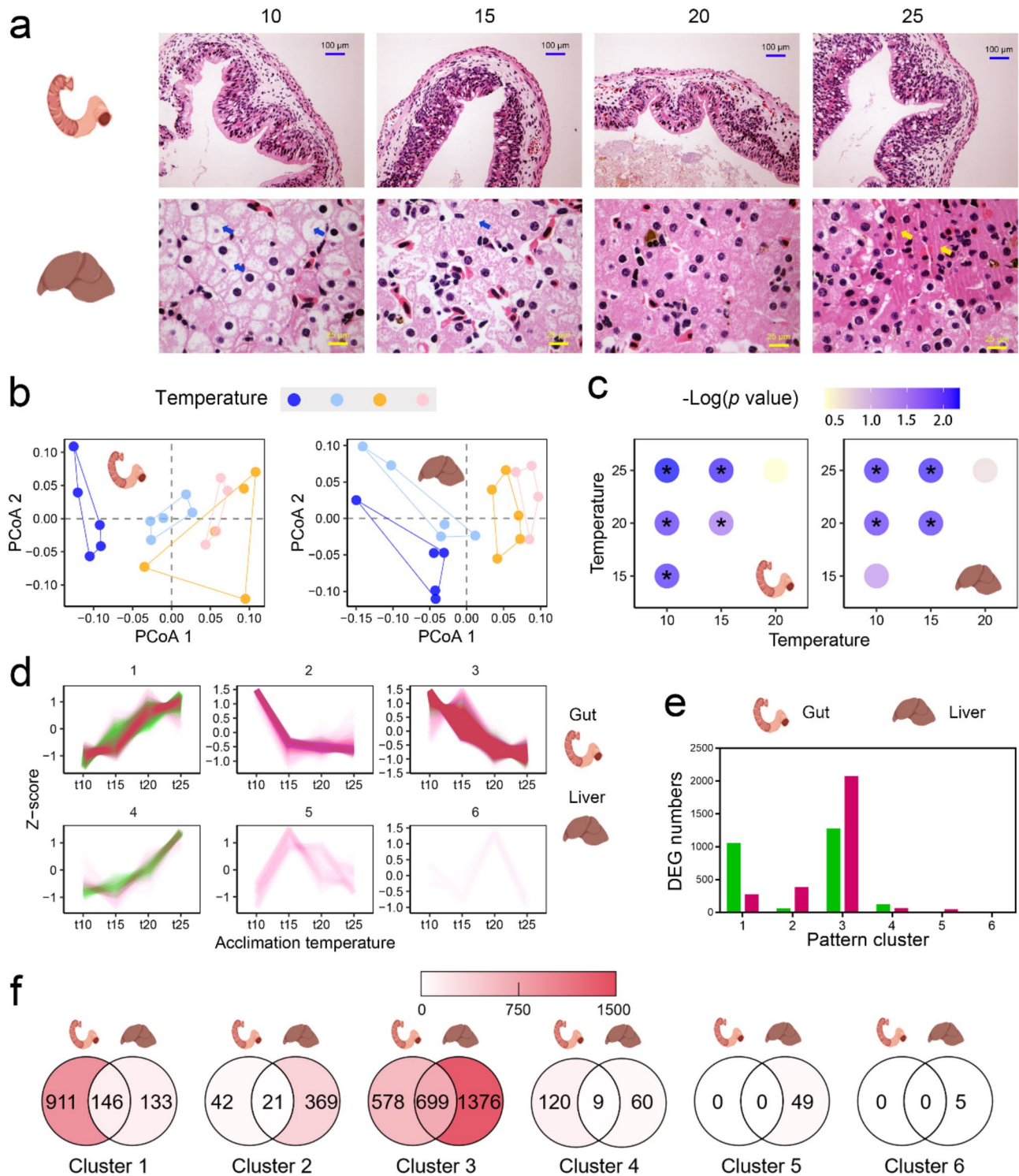


**Fig. 4** Effects of heat stress on gene transcriptional profiles in the gut and liver. **(a)** Histological morphology of gut and liver tissues. The vacuoles in the hepatocytes represent lipid droplets, indicated by blue arrows, while yellow arrows highlight abnormal cellular morphology. **(b)** PCoA scatter plots showing the similarity in gene transcriptional profiles (Bray-Curtis distances) between gut and liver samples. **(c)** Heatmaps presenting the results of pairwise intergroup PERMANOVA on gene transcriptional profiles (Bray-Curtis distances). Asterisks indicate significant differences between groups ( $p < 0.05$ ; pairwise PERMANOVA). **(d)** Variation patterns of differentially expressed genes (DEGs, adjusted  $p < 0.01$ , one-way ANOVA with BH correction). The DEGs were divided into six clusters (Clusters 1–6), each displaying a distinct variation pattern with acclimation temperature. **(e)** Number of DEGs corresponding to each pattern in each tissue. **(f)** Overlap of DEG profiles between the liver and gut for each cluster

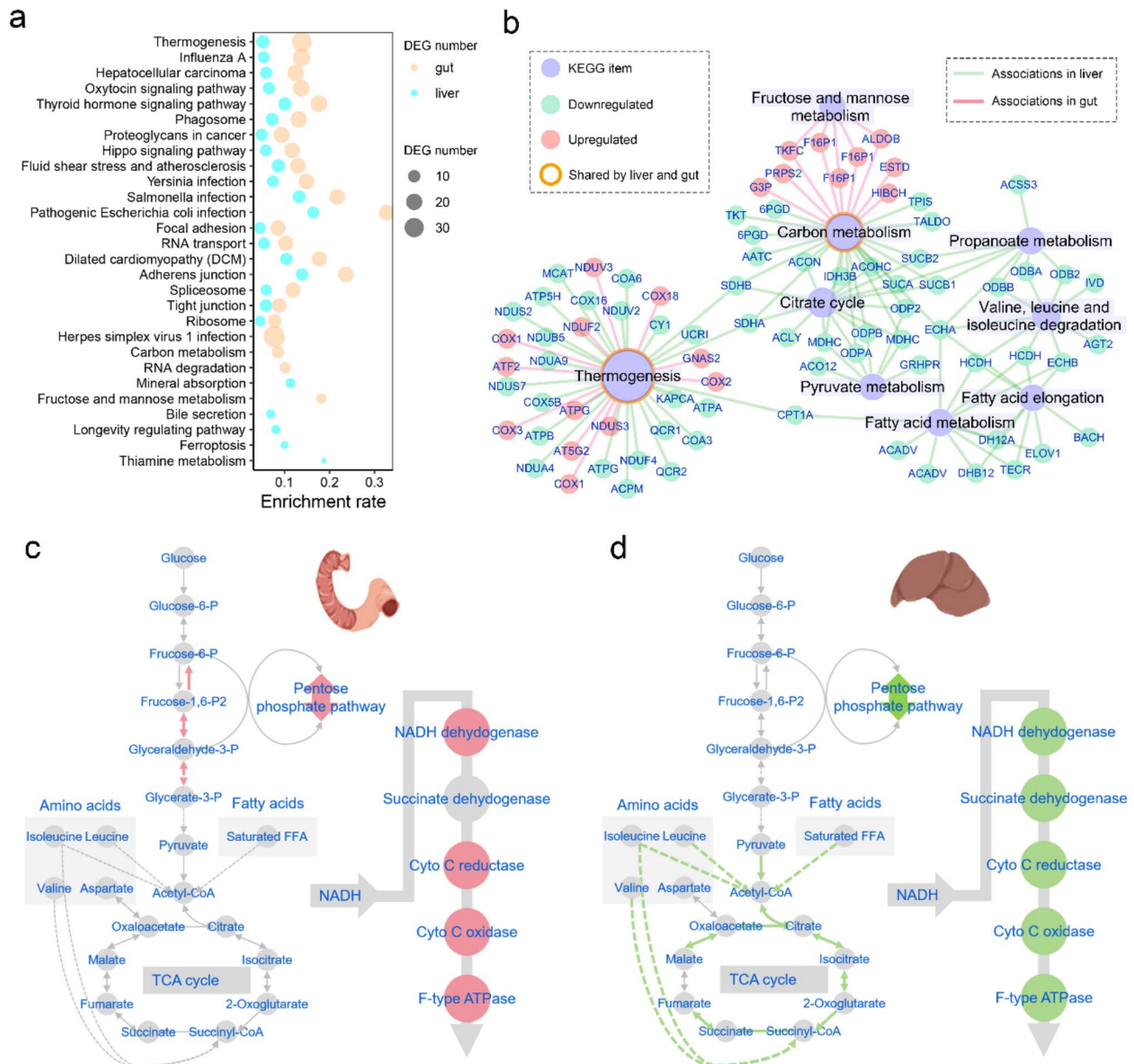


**Fig. 5** Metabolic reorganization of the gut and liver under heat stress. **(a)** KEGG pathways enriched by DEGs with increased transcription in response to rising temperatures (Clusters 1 and 4). **(b)** Network illustrating the metabolic pathways enriched by DEGs with temperature-dependent transcriptional variation (Clusters 3, 1, and 4). **(c–d)** Transcriptional regulation of core substrate and energy metabolic pathways. Red denotes increased transcription, and green denotes decreased transcription with rising temperatures

reticulum, ubiquitin-mediated proteolysis, tight junctions, and the cell cycle (Figure S3), most of which are involved in the central dogma. Heat shock proteins (HSPs) occupied central roles in the sub-networks shared by the liver and gut. The cellular pathways exclusively enriched in the liver included thermogenesis, carbon metabolism, the citrate cycle, propanoate metabolism, pyruvate metabolism, fatty acid metabolism, fatty acid elongation, and amino acid degradation (Fig. 5b and S2b).

To more intuitively present the transcriptional regulation of metabolic fluxes in the liver and gut, we mapped

the DEGs onto the primary metabolic pathways (Fig. 5c–d). The results revealed that the gut exhibited upregulation of some critical genes of gluconeogenesis, pentose phosphate pathway (PPP), and oxidative phosphorylation (OPP) under heat stress, whereas the liver showed downregulation of another groups of genes involved in lipid degradation, amino acid degradation, the citrate cycle, and OPP under heat stress (Figure S4–6). These findings suggest opposing transcriptional adjustments in substrate and energy metabolism between the gut and liver.

## Discussion

Heat stress impaired the somatic growth of CGS and resulted in significant mortality within 30 days at temperatures as low as 20 °C (Fig. 1b–d). These findings underscored the extreme heat sensitivity of these animals. As expected, heat stress affected the liver, gut, and gut microbiota of CGS. However, the gut microbiota were functionally more stable in response to heat stress compared to their composition, and the liver and gut showed remarkable differences in response to elevated temperatures at both histological and transcriptional levels. In the following discussion, we will explore the physiological mechanisms underlying CGS heat sensitivity and the role of the gut–liver axis in this process.

### Liver is a critical organ contributing to the heat susceptibility of CGS

We previously reported that heat-stressed CGS exhibited symptoms such as liver enlargement, glycogen accumulation, and energy deficiency [23], which are reminiscent of human glycogen storage diseases [73]. Under these conditions, lipid and amino acids were depleted to meet energy demands, suggesting that a lipid- and protein-rich diet could mitigate the growth suppression caused by heat stress. Consistent with these observations, we found a temperature-dependent decrease in lipid storage within CGS hepatocytes, indicative of metabolic exhaustion under heat stress (Fig. 4a). Additionally, the compressed hepatocytes observed in the livers of the 25 °C group is a common pathological feature of diseased human livers [74]. These findings highlight the liver as a heat-sensitive organ in CGS.

As temperatures rise, ectotherms are likely to experience increased energy expenditure to maintain cellular homeostasis. This phenomenon was observed in CGS, where the oxygen consumption rate increased with temperature within the range of 7–25 °C [20]. Consistent with this, we demonstrated transcriptional upregulation of oxidative phosphorylation (OPP) in the brain, skin, limbs, and gut under heat stress ([23] and this study). In contrast, the liver of heat-stressed CGS exhibited downregulation of OPP and the upstream substrate catabolism, which contradicts the elevated oxygen consumption (Fig. 5c, S4–S6). This paradox suggests that the liver prioritizes energy conservation under heat stress, likely as a protective strategy in response to nutrient depletion. Furthermore, the observed depletion of hepatic lipids and histological changes, such as hepatocyte compression, support the notion of metabolic exhaustion. Compared to other organs, the liver's energy metabolism appears to be more susceptible to heat stress, potentially limiting the overall heat tolerance of CGS.

### The role of gut microbiota in the heat susceptibility of CGS

Consistent with our previous study [21], heat stress reduced the alpha-diversity of CGS gut microbiota and reorganized their community structure (Fig. 2c–e). The most notable compositional change in the gut microbiota of heat-stressed groups was the decrease in the relative abundance of Actinomycetota and several associated taxa, including *Micrococcaceae*, *Actinomycetaceae*, and *Cellulomonas* (Fig. 2f–g). *Actinomycetota* and *Actinomycetaceae* are known sources of many antibiotics [75, 76], while members of *Cellulomonas* are reported to produce enzymes with cellulolytic, chitinolytic, and cellulolytic activities [77, 78]. Despite these compositional changes, microbial function remained relatively stable. It is important to note that the significant intergroup differences in the metagenome at the unigene level likely reflect differences in microbial composition, as unigenes are assembled independently for each sample before being merged into a common unigene pool (Fig. 3b–c). In this context, orthologous genes from microbes with closer phylogenetic relationships are more likely to be merged into a single unigene, contributing to the observed similarity in the metagenome at the unigene level. When the metagenomes were analyzed at the functional gene or functional pathway levels, the intergroup differences were less pronounced, with no significant pairwise differences detected (Fig. 3d–e). These results suggest that changes in gut microbiota were not likely a major driver of heat susceptibility in CGS (Fig. 6). Distinct differences in how gut microbial composition and function respond to environmental changes are common in animals [79, 80]. Multifunctional redundancy is an intrinsic property of the gut microbiota [81], which may explain the functional stability observed in our study. Maintaining functional redundancy in the gut microbiota could be a crucial adaptive strategy for CGS to survive in varying environments. However, despite this functional stability, the potential implications of compositional changes in gut microbiota should not be overlooked, particularly when shifts in the relative abundance of opportunistic pathogens occur. Such compositional changes may disrupt the delicate balance between the host's immune system and gut microbes, potentially leading to biological consequences by altering the host's immune status [82].

### The role of gut in the heat susceptibility of CGS

The gut and liver showed continuous, gradual transcriptomic changes with rising temperatures, exhibiting progressive alterations across the four temperature conditions (Fig. 4b–c, S1). When focusing on specific variation patterns and gene functions, the two organs demonstrated both similarities and notable differences in their responses to temperature. A significant number of downregulated genes were shared between the gut and

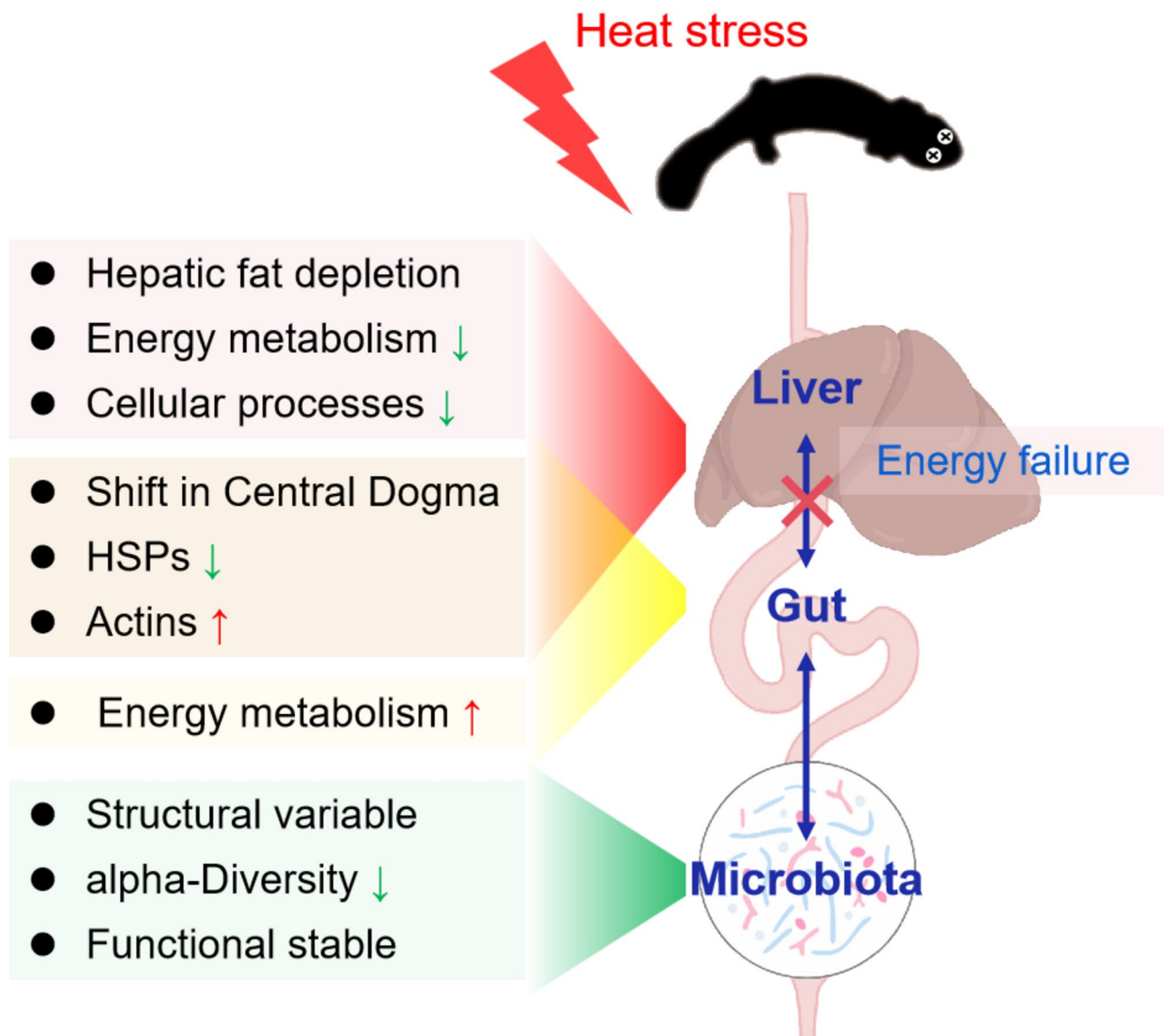


**Fig. 6** A schematic diagram summarizing the results. The opposing transcriptional changes in energy metabolism between the gut and liver suggest that the gut-liver axis is unlikely to be a major pathway contributing to energy failure in CGS under heat stress

liver (Fig. 4f). Heat stress is known to trigger the repression of thousands of genes and the induction of hundreds across different animal species, with downregulated genes consistently outnumbering upregulated ones ([23, 83–85] and this study). Heat stress most significantly impacted five major cellular processes at the transcriptional level: the heat shock response, cytoskeleton, oxidative stress, RNA processing and protein translation, and the cell cycle [86]. This is also the case in CGS. Their gut and liver exhibited similar regulatory patterns for heat shock proteins (HSPs) and actins, a major component of the cytoskeleton. HSPs are ubiquitous protein families that are transcriptionally activated to maintain cellular proteostasis and protect cells under various stresses, such as heat, hypoxia, and endotoxins [87]. Surprisingly,

we observed a downregulation of HSPs in the gut and liver of heat-stressed individuals. One possible explanation for this is the extended duration of thermal acclimation in this study. While transcription is an important regulatory mechanism for HSP expression, it is not the only one [88], and transcriptional upregulation is often observed at the early stages of stress [86]. It is plausible that post-transcriptional regulation serves as the primary mechanism for maintaining HSP levels after prolonged heat stress in CGS. In contrast to HSPs, actin transcription was upregulated in heat-stressed CGS (Figure S2). Recent studies have highlighted the actin cytoskeleton as a key mediator of stress responses [89], with transcriptional activation occurring under heat stress [86]. During acute cellular stress, maintaining the integrity of the

actin cytoskeleton is crucial for the organism's survival, potentially facilitating an HSP-independent pathway that enhances thermotolerance and extends lifespan [90]. Thus, transcriptional activation of actins may be a common protective strategy across organs in CGS. In addition to HSPs and actins, transcriptional changes related to the central dogma were also consistent between the gut and liver. However, their significance in the response of CGS to heat stress remains complex and requires further investigation.

The transcriptional response to heat stress differs markedly between the gut and liver. In the liver, downregulated genes at high temperatures dominate the differentially expressed genes (DEGs), leading to an overall reduction in metabolic activity, likely reflecting an energy conservation mechanism. In contrast, the gut exhibits a more dynamic response, with a relatively higher proportion of upregulated genes under heat stress. This suggests that the gut actively modulates its metabolic pathways to sustain physiological functions, whereas the liver shifts toward energy preservation. Temperature-induced transcriptional changes can result from both proactive regulation and passive effects. Given that RNA transcription is energy-intensive and energy budget is tighter at higher temperatures, gene activation is more likely to reflect an organ's metabolic demands rather than a universal adaptive response. In this context, the gut appears to sustain transcriptional activity in pathways associated with energy production and cellular homeostasis, while the liver downregulates key metabolic processes, possibly as a protective shift toward energy conservation. This contrast suggests that under heat stress, the gut remains metabolically active, whereas the liver adopts an energy-saving strategy, highlighting distinct physiological adjustments beyond a simple proactive-passive classification. Functionally, the most notable differences between the two organs were observed in substrate metabolism and oxidative phosphorylation (OPP). Unlike the liver, the gut showed transcriptional upregulation of glycolysis/gluconeogenesis, the pentose phosphate pathway (PPP), and OPP (Fig. 5a–b and d, S4–S6). The PPP is crucial for ribonucleotide synthesis and is a major source of NADPH, playing a key role in helping cells meet their anabolic demands [91]. Robust PPP and OPP activity are typically associated with rapid somatic growth and favorable nutrient conditions in amphibian larvae [92, 93], in the context of heat stress, this may reflect an effort to maintain cellular homeostasis rather than a purely growth-promoting state. Additionally, the absence of histological deterioration in the gut suggests that it retains structural integrity despite metabolic adjustments (Fig. 4a). These findings indicate that the gut employs a different metabolic strategy than the liver, prioritizing functional resilience rather than energy conservation.

In summary, our results suggest that the liver is more passively affected by heat stress compared to the gut and gut microbiota in CGS. This indicates that thermal effects on the gut-liver axis are unlikely to be a major upstream factor in mediating the heat susceptibility of the liver and the organism as a whole (Fig. 6). As a primary energy storage organ in amphibian larvae [94], the liver's heat intolerance in CGS may be attributed to two main factors: the thermal properties of organ-specific glyco-metabolic enzymes [23] and the increased metabolic demands of other organs, which strain the overall metabolic budget. In this light, maintaining the compositional stability of the gut microbiota may not be a feasible strategy to improve CGS's heat tolerance. Instead, optimizing the nutritional composition and bioavailability of its feed may be a more effective approach to enhancing CGS's heat tolerance. Additionally, our study reaffirms that CGS's heat sensitivity may be intrinsic, underscoring the importance of carefully considering both current and future climate conditions in their conservation efforts.

This study has several limitations. First, we focused exclusively on the thermal performance of CGS larvae, overlooking potential ontogenetic changes in thermal physiological traits. Specifically, we did not account for variations in thermal performance related to age and body weight, which likely influence the individuals' energy status. As a result, our conclusions are limited to CGS larvae and cannot be directly extrapolated to adults. Second, it is important to note that our study is based solely on the Shanxi clade, and whether the findings can be generalized to CGS as a whole requires further investigation. Third, given the high variability of microbiome data and the influence of individual factors such as body condition and sex, the current group sample size may be underpowered to detect reliable patterns. We recognize this limitation and will address it by including larger sample sizes and more individual-level data in future studies.

## Conclusion

In this study, we investigated the potential role of the gut-liver axis in influencing the heat susceptibility of CGS, using a combination of histological analysis, gut metagenomics, and multi-tissue transcriptomics. Our findings indicate that hepatic heat susceptibility plays a central role in CGS's overall heat intolerance. In contrast, the functional profile of the gut microbiota and metabolic capacity of the gut appeared to be less susceptible to heat stress, suggesting that the gut-liver axis may not significantly contribute to their heat susceptibility. Consequently, future research should examine whether the observed metabolic adaptations to prolonged heat stress are reversible or represent long-term physiological adjustments. Additionally, targeted dietary interventions should be experimentally evaluated for their potential to

enhance thermal resilience [95, 96]. Furthermore, investigating the genetic and developmental factors contributing to individual differences in heat susceptibility could provide valuable insights for conservation strategies and captive management. Addressing these aspects would advance our understanding of thermal adaptation in ectotherms and support conservation efforts to mitigate the impacts of climate change on amphibian populations.

### Supplementary Information

The online version contains supplementary material available at <https://doi.org/10.1186/s12864-025-11644-4>.

Supplementary Material 1

### Acknowledgements

We thank Ma Shun, Hanqi Li, and Cheng Shen for their help in sample collection.

### Author contributions

Conceptualization, R.-L.Z., W.Z., C.-L.Z., L.-M.C., and J.-P.J.; methodology, R.-L.Z., W.Z., C.-L.Z., L.-M.C., and T.Z.; software, R.-L.Z., C.-L.Z., J.-Y.L., and L.-M.C.; formal analysis, W.Z., R.-L.Z., C.-L.Z., L.-M.C., and J.-Y.L.; investigation, W.Z., R.-L.Z., C.-L.Z., L.-M.C., and J.-Y.L.; resources, W.Z., R.-L.Z., C.-L.Z., L.-M.C., T.Z., and J.-P.J.; data curation, W.Z. and R.-L.Z.; writing—original draft preparation, W.Z., R.-L.Z., C.-L.Z., and L.-M.C.; writing—review and editing, W.Z., R.-L.Z., C.-L.Z., L.-M.C., J.-Y.L., T.Z., and J.-P.J.; visualization, W.Z. and R.-L.Z.; supervision, J.-P.J. and W.Z.; project administration, W.Z. and J.-P.J.; funding acquisition, W.Z. and J.-P.J. All authors participated in the manuscript preparation and approved the final version of the manuscript.

### Funding

This work was supported by National Natural Science Foundation of China (Grant no. 32370529 and 31900327), Natural Science Foundation of Sichuan Province of China (Grant no. 2023NSFSC1153), the Fundamental Research Funds for the Central Universities (Grant No. SWU-KR24004), and China Biodiversity Observation Networks (Sino BON-Amphibian & Reptile).

### Data availability

The raw sequencing data generated in this study have been deposited in the Genome Sequence Archive (GSA). The metagenomic data are accessible under accession number CRA018593 at <https://bigd.big.ac.cn/gsa/browse/CRA018593>, and the transcriptomic data are available under accession number CRA016012 at <https://bigd.big.ac.cn/gsa/browse/CRA016012>.

### Declarations

#### Ethics approval and consent to participate

All animal protocols in this study were reviewed and approved by the Animal Ethical and Welfare Committee of the Chengdu Institute of Biology, Chinese Academy of Sciences (permit number: CIBDWLL2023013), in compliance with the ARRIVE guidelines 2.0 and the Guide for the Care and Use of Laboratory Animals (8th edition) published by the National Research Council (US) Committee for the Update of the Guide for the Care and Use of Laboratory Animals.

#### Consent for publication

Not applicable.

#### Competing interests

The authors declare no competing interests.

Received: 24 October 2024 / Accepted: 28 April 2025

Published online: 13 May 2025

### References

1. Jørgensen LB, Ørsted M, Malte H, Wang T, Overgaard J. Extreme escalation of heat failure rates in ectotherms with global warming. *Nature*. 2022;611(7934):93–8.
2. Deutsch CA, Tewksbury JJ, Huey RB, Sheldon KS, Ghalambor CK, Haak DC, Martin PR. Impacts of climate warming on terrestrial ectotherms across latitude. *Proceedings of the National Academy of Sciences* 2008, 105(18):6668–6672.
3. Luedtke JA, Chanson J, Neam K, Hobin L, Maciel AO, Catenazzi A, Borzée A, Hamidy A, Aowphol A, Jean A, et al. Ongoing declines for the world's amphibians in the face of emerging threats. *Nature*. 2023;622(7982):308–14.
4. Alan Pounds J, Bustamante MR, Coloma LA, Consuegra JA, Fogden MPL, Foster PN, La Marca E, Masters KL, Merino-Viteri A, Puschendorf R, et al. Widespread amphibian extinctions from epidemic disease driven by global warming. *Nature*. 2006;439(7073):161–7.
5. Alford RA, Bradfield KS, Richards SJ. Global warming and amphibian losses. *Nature*. 2007;447(7144):E3–4.
6. D'Amen M, Bombi P. Global warming and biodiversity: evidence of climate-linked amphibian declines in Italy. *Biol Conserv*. 2009;142(12):3060–7.
7. Gonzalez-Rivas PA, Chauhan SS, Ha M, Fegan N, Dunshea FR, Warner RD. Effects of heat stress on animal physiology, metabolism, and meat quality: A review. *Meat Sci*. 2020;162:108025.
8. Hofmann GE, Todgham AE. Living in the now: physiological mechanisms to tolerate a rapidly changing environment. *Annu Rev Physiol*. 2010;72:127–45.
9. Shu GC, Liu P, Zhao T, Li C, Hou YM, Zhao CL, Wang J, Shu XX, Chang J, Jiang JP, et al. Disordered translocation is hastening local extinction of the Chinese giant salamander. *Asian Herpetological Res*. 2021;12:271–9.
10. Yan F, Lü J, Zhang B, Yuan Z, Zhao H, Huang S, Wei G, Mi X, Zou D, Xu W, et al. The Chinese giant salamander exemplifies the hidden extinction of cryptic species. *Curr Biol*. 2018;28(10):R590–2.
11. Gao KQ, Shubin NH. Earliest known crown-group salamanders. *Nature*. 2003;422(6930):424–8.
12. Wang J, Zhang HX, Xie F, Wei G, Jiang JP. Genetic bottlenecks of the wild Chinese giant salamander in karst caves. *Asian Herpetological Res*. 2017;8:174–83.
13. Fei L, Hu SQ, Ye CY, Huang YZ. *Fauna Sinica, Amphibia vol. 1, Amphibia gymnophiona and Urodela*. Beijing: Science; 2006.
14. Zhao T, Zhang WY, Zhou J, Zhao CL, Liu XK, Liu ZD, Shu GC, Wang SS, Li C, Xie F, et al. Niche divergence of evolutionarily significant units with implications for repopulation programs of the world's largest amphibians. *Sci Total Environ*. 2020;738:140269.
15. Jiang JP, Xie F, Li C, Wang B. *China's red list of biodiversity: vertebrates vol. IV, amphibians*. Beijing: Science; 2021.
16. IUCN SSC Amphibian Specialist Group. 2023. *Andrias davidianus*. The IUCN Red List of Threatened Species 2023: e.T179010104A48438418 <https://dx.doi.org/10.2305/IUCN.UK.2023-1.RLTS.T179010104A48438418.en>
17. Lu C, Chai J, Murphy RW, Che J. Giant salamanders: farmed yet endangered. *Science*. 2020;367(6481):989.
18. Hu QM, Tian HF, Xiao HB. Effects of temperature and sex steroids on sex ratio, growth, and growth-related gene expression in the Chinese giant salamander *Andrias davidianus*. *Aquat Biology*. 2019;28:79–90.
19. Zhang L, Kouba A, Wang QJ, Zhao H, Jiang W, Willard S, Zhang HX. The effect of water temperature on the growth of captive Chinese giant salamanders (*Andrias davidianus*) reared for reintroduction: A comparison with wild salamander body condition. *Herpetologica*. 2014;70(4):369–77.
20. Zhao CL, Zhao T, Feng JY, Chang LM, Zheng PY, Fu SJ, Li XM, Yue BS, Jiang JP, Zhu W. Temperature and diet acclimation modify the acute thermal performance of the largest extant amphibian. *Animals*. 2022;12(4):531.
21. Zhu LF, Zhu W, Zhao T, Chen H, Zhao CL, Xu LL, Chang Q, Jiang JP. Environmental temperatures affect the Gastrointestinal microbes of the Chinese giant salamander. *Front Microbiol*. 2021;12:543767.
22. Zhu W, Zhao CL, Zhao T, Chang LM, Chen QH, Liu JY, Li C, Xie F, Jiang JP. Rising floor and dropping ceiling: organ heterogeneity in response to cold acclimation of the largest extant amphibian. *Proc R Soc B* 2022;(289):20221394.
23. Zhu W, Zhao T, Zhao CL, Li C, Xie F, Liu JY, Jiang JP. How will warming affect the growth and body size of the largest extant amphibian? More than the temperature-size rule. *Sci Total Environ*. 2022;859(Pt 1):160105.
24. Chen XB, Shen JZ, Zhao JY, Xiong JJ, Zhang GL. The effect of water temperature on intake of *Andrias davidianus* (in Chinese). *Fish Sci*. 1999;1:20–2.
25. Mu HM, Li Y, Yao JK, Ma S. A review: current research on biology of Chinese giant salamander. *Fish Sci*. 2011;30(8):513–6.

26. Wang HW. The artificial culture of Chinese giant salamander. *J Aquaculture*. 2004;25(5):41–4.
27. Zhang Z, Mammola S, Liang Z, Capinha C, Wei Q, Wu Y, Zhou J, Wang C. Future climate change will severely reduce habitat suitability of the critically endangered Chinese giant salamander. *Freshw Biol*. 2020;65(5):971–80.
28. Wang JH, Zhang L, Zhang PJ, Sun B J. Physiological processes through which heatwaves threaten fauna biodiversity. *The Innovation Life* 2024, 2(2).
29. Zhu W, Qi Y, Wang XY, Shi XD, Chang LM, Liu JY, Zhu LF, Jiang JP. Multi-omics approaches revealed the associations of host metabolism and gut Microbiome with phylogeny and environmental adaptation in mountain Dragons. *Front Microbiol*. 2022;13:913700.
30. Hsu CL, Schnabl B. The gut–liver axis and gut microbiota in health and liver disease. *Nat Rev Microbiol*. 2023;21(11):719–33.
31. Delzenne NM, Knudsen C, Beaumont M, Rodríguez J, Neyrinck AM, Bindels LB. Contribution of the gut microbiota to the regulation of host metabolism and energy balance: a focus on the gut–liver axis. *Proceedings of the Nutrition Society* 2019, 78(3):319–328.
32. Rooks MG, Garrett WS. Gut microbiota, metabolites and host immunity. *Nat Rev Immunol*. 2016;16(6):341–52.
33. Hooper LV, Littman DR, Macpherson AJ. Interactions between the microbiota and the immune system. *Science*. 2012;336:1268.
34. Sonnenburg JL, Backhed F. Diet-microbiota interactions as moderators of human metabolism. *Nature*. 2016;535(7610):56–64.
35. Tremaroli V, Bäckhed F. Functional interactions between the gut microbiota and host metabolism. *Nature*. 2012;489(7415):242–9.
36. Ringseis R, Gessner DK, Eder K. The gut–liver axis in the control of energy metabolism and food intake in animals. *Annu Rev Anim Biosci*. 2020;8:295–319.
37. Fontaine SS, Mineo PM, Kohl KD. Experimental manipulation of microbiota reduces host thermal tolerance and fitness under heat stress in a vertebrate ectotherm. *Nat Ecol Evol*. 2022;6(4):405–17.
38. Zhang XY, Sukhchuluun G, Bo TB, Chi QS, Yang JJ, Chen B, Zhang L, Wang DH. Huddling remodels gut microbiota to reduce energy requirements in a small mammal species during cold exposure. *Microbiome*. 2018;6(1):103.
39. Bo TB, Zhang XY, Wen J, Deng K, Qin XW, Wang DH. The microbiota–gut–brain interaction in regulating host metabolic adaptation to cold in male Brandt’s voles (*Lasiodopodmys brandtii*). *ISME J*. 2019;13(12):3037–53.
40. Kearney M, Shine R, Porter WP. The potential for behavioral thermoregulation to buffer cold-blooded animals against climate warming. *Proc Natl Acad Sci*. 2009;106(10):3835–40.
41. Percie du Sert N, Ahluwalia A, Alam S, Avey MT, Baker M, Browne WJ, Clark A, Cuthill IC, Dirnagl U, Emerson M, et al. Reporting animal research: explanation and elaboration for the ARRIVE guidelines 2.0. *PLoS Biol*. 2020;18(7):e3000411.
42. National Research Council (US). Committee for the update of the guide for the care and use of laboratory animals: guide for the care and use of laboratory animals. Washington (DC): National Academies Press (US); 2011.
43. Chen TT, Chen X, Zhang SS, Zhu JW, Tang BX, Wang A, Dong LL, Zhang ZW, Yu CX, Sun YL, et al. The genome sequence archive family: toward explosive data growth and diverse data types. *Genom Proteom Bioinform*. 2021;19(4):578–83.
44. Members CN, Partners. Database resources of the National genomics data center, China National center for bioinformatics in 2022. *Nucleic Acids Res*. 2021;50(D1):D27–38.
45. Bolger AM, Lohse M, Usadel B. Trimmomatic: a flexible trimmer for illumina sequence data. *Bioinformatics*. 2014;30(15):2114–20.
46. FastQC. a quality control tool for high throughput sequence data.
47. Ewels P, Magnusson M, Lundin S, Käller M. MultiQC: summarize analysis results for multiple tools and samples in a single report. *Bioinf (Oxford England)*. 2016;32(19):3047–8.
48. Li D, Luo R, Liu CM, Leung CM, Ting HF, Sadakane K, Yamashita H, Lam TW. MEGAHIT v1.0: a fast and scalable metagenome assembler driven by advanced methodologies and community practices. *Methods*. 2016;102:3–11.
49. Gurevich A, Saveliev V, Vyahhi N, Tesler G. QUAST: quality assessment tool for genome assemblies. *Bioinformatics*. 2013;29(8):1072–5.
50. Hyatt D, Chen GL, LoCascio PF, Land ML, Larimer FW, Hauser LJ. Prodigal: prokaryotic gene recognition and translation initiation site identification. *BMC Bioinformatics*. 2010;11(1):119.
51. Mirdita M, Steinegger M, Breitwieser F, Söding J, Levy Karin E. Fast and sensitive taxonomic assignment to metagenomic contigs. In: *bioRxiv*; 2020.
52. Li H. Aligning sequence Reads, clone sequences and assembly contigs with BWA-MEM. *ArXiv* 2013; 1303.3997. <https://arxiv.org/abs/1303.3997>
53. Coordinators NR. Database resources of the National center for biotechnology information. *Nucleic Acids Res*. 2017;46(D1):D8–13.
54. Huerta-Cepas J, Szklarczyk D, Heller D, Hernández-Plaza A, Forslund SK, Cook H, Mende DR, Letunic I, Rattei T, Jensen Lars J, et al. EggNOG 5.0: a hierarchical, functionally and phylogenetically annotated orthology resource based on 5090 organisms and 2502 viruses. *Nucleic Acids Res*. 2018;47(D1):D309–14.
55. Kanehisa M, Goto S, Sato Y, Furumichi M, Tanabe M. KEGG for integration and interpretation of large-scale molecular data sets. *Nucleic Acids Res*. 2011;40:D109–14.
56. Terrapon N, Lombard V, Drula E, Coutinho PM, Henrissat B. The CAZy database: principles and usage guidelines. In: 2017; 2017.
57. Alcock BP, Raphenya AR, Lau TTY, Tsang KK, Bouchard M, Edalatmand A, Huynh W, Nguyen A-LV, Cheng AA, Liu S, et al. CARD 2020: antibiotic resistance surveillance with the comprehensive antibiotic resistance database. *Nucleic Acids Res*. 2019;48:D517–25.
58. Liu B, Zheng DD, Jin Q, Chen LH, Yang J. VFDB 2019: a comparative pathogenomic platform with an interactive web interface. *Nucleic Acids Res*. 2018;47:D687–92.
59. Urban M, Cuzick A, Seager J, Wood V, Rutherford K, Venkatesh SY, De Silva N, Martinez MC, Pedro H, Yates AD, et al. PHI-base: the pathogen–host interactions database. *Nucleic Acids Res*. 2019;48(D1):D613–20.
60. Wood DE, Lu J, Langmead B. Improved metagenomic analysis with kraken 2. *Genome Biol*. 2019;20(1):257.
61. O’Leary NA, Wright MW, Brister JR, Ciufu S, Haddad D, McVeigh R, Rajput B, Robbertse B, Smith-White B, Ako-Adjei D, et al. Reference sequence (RefSeq) database at NCBI: current status, taxonomic expansion, and functional annotation. *Nucleic Acids Res*. 2016;44(D1):D733–745.
62. Langmead B, Salzberg SL. Fast gapped-read alignment with bowtie 2. *Nat Methods*. 2012;9(4):357–9.
63. Grabherr MG, Haas BJ, Yassour M, Levin JZ, Thompson DA, Amit I, Adiconis X, Fan L, Raychowdhury R, Zeng Q, et al. Full-length transcriptome assembly from RNA-Seq data without a reference genome. *Nat Biotechnol*. 2011;29(7):644–52.
64. Davidson NM, Oshlack A. Corset: enabling differential gene expression analysis for de novo assembled transcriptomes. *Genome Biol*. 2014;15(7):410.
65. Patro R, Duggal G, Love MI, Irizarry RA, Kingsford C. Salmon provides fast and bias-aware quantification of transcript expression. *Nat Methods*. 2017;14(4):417–9.
66. Simão FA, Waterhouse RM, Ioannidis P, Kriventseva EV, Zdobnov EM. BUSCO: assessing genome assembly and annotation completeness with single-copy orthologs. *Bioinformatics*. 2015;31(19):3210–2.
67. R Core Team. R: a language and environment for statistical computing. *R Foundation for Statistical Computing, Vienna, Austria* 2021.
68. Dixon P. VEGAN, a package of R functions for community ecology. *J Veg Sci*. 2003;14(6):927–30.
69. Liu C, Cui YM, Li XZ, Yao MJ. Microeco: an R package for data mining in microbial community ecology. *FEMS Microbiol Ecol*. 2021;97(2):fiaa255.
70. Wu M, Gu L. TCseq: Time course sequencing data analysis. *R package version 1.280* 2024.
71. Xie C, Mao X, Huang J, Ding Y, Wu J, Dong S, Kong L, Gao G, Li CY, Wei L. KOBAS 2.0: a web server for annotation and identification of enriched pathways and diseases. *Nucleic Acids Res*. 2011;39(suppl2):W316–22.
72. Wickham H. ggplot2: elegant graphics for data analysis, 2nd edition edn. New York: Springer; 2016.
73. Özen HJWW. Glycogen storage diseases: new perspectives. *World J Gastroenterol*. 2007;13(18):2541.
74. Sonthalia N, Jain S, Pawar S, Zanwar V, Surude R. Rathi PMJWjoh: primary hepatic amyloidosis: a case report and review of literature. *World J Hepatol*. 2016, 8(6):340.
75. Millán-Aguñaga N, Soldatou S, Brozio S, Munnoch JT, Howe J, Hoskisson PA, Duncan KR. Awakening ancient Polar actinobacteria: diversity, evolution and specialized metabolite potential. *Microbiology*. 2019;165(11):1169–80.
76. van Bergeijk DA, Augustijn HE, Elsayed SS, Willemsse J, Carrión VJ, Du C, Urem M, Grigoreva LV, Cheprasov MY, Grigoriev S, et al. Taxonomic and metabolic diversity of actinomycetota isolated from faeces of a 28,000-year-old mammoth. *Environ Microbiol*. 2024;26(2):e16589.
77. Sun XX, Li JJ, Du J, Xiao HH, Ni JF. *Cellulomonas macrotermitis* Sp. nov., a chitinolytic and cellulolytic bacterium isolated from the hindgut of a fungus-growing termite. *Antonie Van Leeuwenhoek*. 2018;111(3):471–8.

78. Batool I, Gulfranz M, Asad MJ, Kabir F, Khadam S, Ahmed AJB. *Cellulomonas* Sp isolated from termite gut for saccharification and fermentation of agricultural biomass. *BioResources*. 2018;13(1):752–63.
79. Li H, Xia WC, Liu XY, Wang XY, Liu GQ, Chen H, Zhu LF, Li DY. Food provisioning results in functional, but not compositional, convergence of the gut Microbiomes of two wild *Rhinopithecus* species: evidence of functional redundancy in the gut Microbiome. *Sci Total Environ*. 2022;858:159957.
80. Zhu W, Chang LM, Zhang MH, Chen QH, Sui LL, Shen C, Jiang JP. Microbial diversity in mountain-dwelling amphibians: the combined effects of host and Climatic factors. *iScience*. 2024;27(6):109907.
81. Moya A, Ferrer M. Functional redundancy-induced stability of gut microbiota subjected to disturbance. *Trends Microbiol*. 2016;24(5):402–13.
82. Zhu W, Zhao CL, Feng JY, Chang J, Zhu WB, Chang LM, Liu JY, Xie F, Li C, Jiang JP, et al. Effects of habitat river Microbiome on the symbiotic microbiota and Multi-Organ gene expression of Captive-Bred Chinese giant salamander. *Front Microbiol*. 2022;13:884880.
83. Vihervaara A, Mahat DB, Guertin MJ, Chu T, Danko CG, Lis JT, Sistonen L. Transcriptional response to stress is pre-wired by promoter and enhancer architecture. *Nat Commun*. 2017;8(1):255.
84. Mahat DB, Salamanca HH, Duarte FM, Danko CG, Lis JT. Mammalian heat shock response and mechanisms underlying its Genome-wide transcriptional regulation. *Mol Cell*. 2016;62(1):63–78.
85. Duarte FM, Fuda NJ, Mahat DB, Core LJ, Guertin MJ, Lis JT. Transcription factors GAF and HSF act at distinct regulatory steps to modulate stress-induced gene activation. *Genes Dev*. 2016;30(15):1731–46.
86. Vihervaara A, Duarte FM, Lis JT. Molecular mechanisms driving transcriptional stress responses. *Nat Rev Genet*. 2018;19(6):385–97.
87. Hu C, Yang J, Qi ZP, Wu H, Wang BL, Zou FM, Mei HS, Liu J, Wang WC, Liu QS. Heat shock proteins: biological functions, pathological roles, and therapeutic opportunities. *MedComm (2020)*. 2022;3(3):e161.
88. Lang BJ, Guerrero ME, Prince TL, Okusha Y, Bonorino C, Calderwood SK. The functions and regulation of heat shock proteins; key orchestrators of proteostasis and the heat shock response. *Arch Toxicol*. 2021;95(6):1943–70.
89. Figard L, Zheng L, Biel N, Xue Z, Seede H, Coleman S, Golding I, Sokac AM. Cofilin-mediated actin stress response is maladaptive in heat-stressed embryos. *Cell Rep*. 2019;26(13):3493–e35013494.
90. Baird NA, Douglas PM, Simic MS, Grant AR, Moresco JJ, Wolff SC, Yates JR, Manning G, Dillin A. HSF-1-mediated cytoskeletal integrity determines thermotolerance and life span. *Science*. 2014, 346(6207):360–3.
91. Patra KC, Hay N. The Pentose phosphate pathway and cancer. *Trends Biochem Sci*. 2014;39(8):347–54.
92. Zhu W, Chang LM, Zhao T, Wang B, Jiang JP. Remarkable metabolic reorganization and altered metabolic requirements in frog metamorphic climax. *Front Zool*. 2020;17:30.
93. Zhu W, Chang LM, Shu GC, Wang B, Jiang JP. Fatter or stronger: resource allocation strategy and the underlying metabolic mechanisms in amphibian tadpoles. *Comp Biochem Physiol Part D Genomics Proteom*. 2021;38:100825.
94. Zhu W, Zhang MH, Chang LM, Li C, Zhu WB, Xie F, Zhang H, Zhao T, Jiang JP. Characterizing the composition, metabolism and physiological functions of the fatty liver in *Rana omeimontis* tadpoles. *Front Zool*. 2019;16:42.
95. Li J, King K. Microbial primer: Microbiome and thermal tolerance - a new frontier in climate resilience? *Microbiol*. 2025, 171(1):001523.
96. Doering T, Wall M, Putschim L, Rattanawongwan T, Schroeder R, Hentschel U, Roik A. Towards enhancing coral heat tolerance: a Microbiome transplantation treatment using inoculations of homogenized coral tissues. *Microbiome*. 2021;9(1):102.

### Publisher's note

Springer Nature remains neutral with regard to jurisdictional claims in published maps and institutional affiliations.